Lasers in Medical Science (2025) 40:472
https://doi.org/10.1007/s10103-025-04735-x

RESEARCH

Enhancing cementoenamel junction (CEJ) imaging using gold nanorods in optical coherence tomography (OCT)

Carolina Pereira Da Silva[1] · Maria Heloísa da Conceição Tavares de Lima[1] · Manoel Bernardo da Silva Júnior[1] · Marcela Rosa Nogueira Cavalcanti[1] · Audrey Nunes de Andrade[2] · Avishek Das[3] et al. ***[full author details at the end of the article]***

Received: 23 August 2025 / Accepted: 4 November 2025

Abstract

This study investigates the innovative use of gold nanorods (AuNRs) as optical clearing agents to enhance detailed visualization of the cementoenamel junction (CEJ) in optical coherence tomography (OCT), a non-invasive imaging modality. Eighty extracted teeth were carefully examined using scanning electron microscopy (SEM) and energy-dispersive X-ray spectroscopy (EDS) to classify CEJ types. Imaging was performed under four distinct contrast conditions: air (G1), glycerol (G2), AuNRs (G3), and AuNRs combined with glycerol (G4). Statistical analysis (ANOVA and Tukey's test, $p < 0.05$) showed that AuNRs, especially in G4, significantly enhanced CEJ visualization by reducing scattering and improving image contrast. Specifically, for the enamel region, the AuNRs-containing groups (G3 and G4) showed the lowest attenuation coefficients (0.0011100 and 0.0010435, respectively), compared to groups 2 and 1. The same was observed in the CEJ region: the AuNRs-containing groups (G3 and G4) showed the lowest attenuation coefficients (0.0010830 and 0.0009060, respectively). Attenuation analysis indicated greater absorption in the enamel and CEJ regions with AuNRs and glycerol, while cementum remained unaffected. The preservation of cementum suggests that the combination of AuNRs and glycerol enhanced OCT imaging without compromising tissue integrity. These results highlight the potential of AuNRs to further enhance OCT-based CEJ imaging for detecting clinically significant "gaps," thereby advancing its role as a reliable diagnostic tool in dentistry.

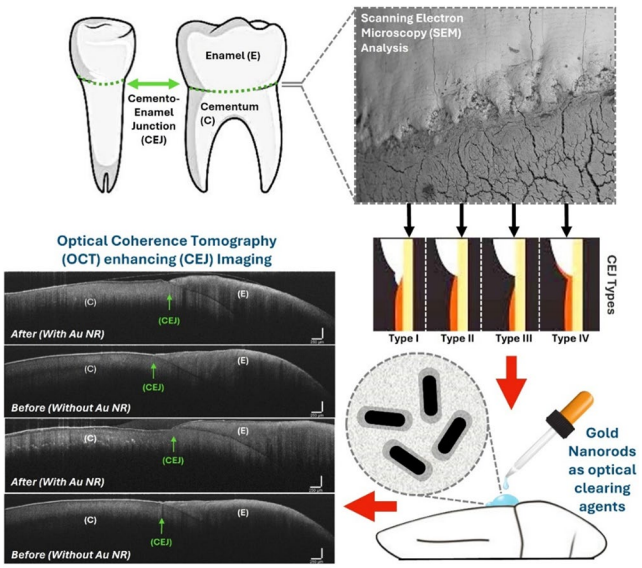

Keywords Cementoenamel junction · Metal nanoparticles or nanotechnology · Optical coherence tomography · Dentistry · Optical imaging

✉

Published online: 10 November 2025

Abbreviations

AuNRs	gold nanorods
CEJ	cementoenamel junction
EDS	energy-dispersive X-ray spectroscopy
OCT	optical coherence tomography
OAC	optical attenuation coefficient
OCAs	optical clearing agents
ROIs	regions of interest
SEM	scanning electron microscopy

Introduction

The cementoenamel junction (CEJ) is a critical anatomical structure in clinical dentistry, serving as a precise reference point for evaluating clinical attachment levels and gingival health [1, 2]. In periodontology, it defines the boundary for root coverage procedures, while in restorative and prosthodontic practice it guides cervical restorations and prosthetic margins. Misidentification of the CEJ can lead to complications such as pain, or root involvement. Therefore, precise CEJ detection is essential for treatment planning and prognosis [3]. Furthermore, exposure or wear of the CEJ can predispose teeth to conditions such as dental caries and failures at restorative interfaces [4], underscoring the importance of this structure for maintaining oral health and informing effective treatment planning [5].

Traditional methods for CEJ assessment include visual inspection, tactile evaluation using periodontal probes, and various imaging techniques, including intraoral radiographs, cone-beam computed tomography (CBCT), and micro-CT [6–8]. Conversely, these approaches introduce clinical constraints, including invasiveness, patient morbidity, and ionizing radiation burden. Methodologically, they are limited by the translation of three-dimensional microanatomy into a two-dimensional projection, leading to compromised spatial resolution and diagnostic fidelity [9].

In contrast, bio-photonic devices, such as optical coherence tomography (OCT) [10], offer a non-destructive alternative for CEJ visualization. OCT operates based on the coherent properties of light, enabling the acquisition of cross-sectional images of biological tissues at depths of up to 3 mm without ionizing radiation. This non-invasive technique holds significant potential for dental applications, including the detection and diagnosis of dental caries, fissures, demineralization [11–13], and other morphological characteristics of dental hard tissues, which remain underexplored in current research.

However, the high degree of light scattering in turbid biological tissues limits the penetration depth, leading to a decrease in both image resolution and contrast as light propagates deeper [14]. This challenge significantly impedes the efficacy of OCT in clinical settings, necessitating the incorporation of optical clearing agents (OCAs) such as nanomaterials [15, 16].

Among these, gold nanorods (AuNRs), with their anisotropic structure, exhibit unique optical property such as localized surface plasmon resonances (LSPRs) that enhance their use as contrast agents for OCT [17]. The plasmon resonance is tunable over a broad range of wavelengths, typically in the near-infrared (NIR) region, which is advantageous for biological imaging as it minimizes tissue absorption and scattering. Their application in dentistry, although relatively recent, shows promise due to their biocompatibility and potential tissue-protective benefits.

Compared with other nanoparticle-based contrast agents, AuNRs offer several unique advantages for OCT imaging. Gold nanospheres and silica nanoparticles provide enhanced scattering, but their isotropic geometry limits spectral tunability in the near-infrared (NIR) window that is optimal for dental tissue imaging [18, 19]. Silver nanoparticles exhibit strong plasmonic activity but raise concerns about cytotoxicity and reduced biocompatibility in biological environments [20]. Quantum dots provide high fluorescence yields but are less effective as scattering agents for OCT and often involve heavy metals, limiting their clinical translation [21]. In contrast, AuNRs possess an anisotropic structure that enables precise tuning of their LSPR into the NIR region, which coincides with the 'optical window' of biological tissues, thereby minimizing absorption and maximizing penetration depth [22, 23].

At resonance, the collective oscillation of conduction electrons amplifies both absorption and scattering, increasing backscattered signal intensity while reducing multiple forward-scattering events that degrade image quality [24]. This property directly enhances contrast at structural interfaces such as the cementoenamel junction, making AuNRs particularly well suited for dental OCT. Moreover, their chemical inertness, relative biocompatibility, and stability under physiological conditions provide additional advantages for clinical translation, while potential limitations such as surfactant (CTAB) toxicity or aggregation can be mitigated by purification and surface modification strategies [25, 26]. Furthermore, these nanoparticles enhance image contrast, facilitating more detailed and accurate visualization of biological structures [19].

By enhancing the absorption and scattering properties of OCT images, the integration of gold nanoparticles improves the overall visualization capabilities of the technique, particularly when coupled with viable contrast agents [18, 27, 28]. Previous studies have explored the use of other optical contrast agents for dental or biomedical

imaging, such as silver nanoparticles and silica nanoparticles. However, these materials present limitations including cytotoxicity, reduced biocompatibility and lower stability [16, 29].

Despite the promise of OCT and the advantageous properties of AuNRs, to date, there is a notable absence of studies investigating the use of gold nanoparticles specifically for enhancing CEJ imaging in the cervical region of the tooth. This gap highlights an unexplored area with significant clinical implications. Given the importance of understanding the integrity of the cementoenamel junction in preventing overtreatment and optimizing periodontal, restorative, and rehabilitative procedures, and recognizing that high-resolution, non-invasive analysis techniques remain underexplored, this study aims to evaluate the potential of AuNRs as optical contrast agents for OCT imaging in the identification of the CEJ.

Materials and methods

Sample preparation

Eighty extracted human premolars and molars were obtained from the Human Tooth Bank at the Tabosa de Almeida University Center (ASCES/UNITA). Teeth with extensive caries, restorations, fractures, or resorptions were excluded. After disinfection, samples were stored in deionized water at 4 °C. Each tooth was embedded in self-curing acrylic resin for stability during imaging.

Gold nanorod (AuNR) preparation

AuNRs were synthesized using the seed-mediated growth method [28]. Initially, sodium oleate (NaOL) was prepared by reacting oleic acid with sodium hydroxide (NaOH) in ethanol, yielding a purified precipitate for subsequent use. The gold seed solution was generated by dissolving $HAuCl_4$ in a cetyltrimethylammonium bromide (CTAB) solution, followed by reduction with $NaBH_4$, leading to a color change indicative of seed formation. The growth solution was prepared by combining CTAB with NaOL, $HAuCl_4$, hydrochloric acid (HCl), and ascorbic acid, with controlled temperature and stirring conditions. The gold seeds were then introduced to the growth medium and left to incubate at 30 °C for 12 h, allowing AuNRs to develop. The final dispersion was centrifuged to remove excess reactants, leaving a purified solution with a distinct purplish color. The AuNRs used in this study had an average length of 68 nm, diameter of 11.7 nm, and an aspect ratio of 5.3.

Scanning electron microscopy (SEM) and energy dispersive x-ray spectroscopy (EDS)

The SEM analysis was conducted using a TM3000 (Hitachi, Japan) at the Lasers and Applications Center – IPEN/USP to characterize the CEJ morphology. The SEM operated at 5 kV for secondary electron imaging and 20 kV for backscattered electron imaging. EDS analysis (Quantax 70, Bruker Corporation) was performed to determine elemental composition in enamel, cementum, and the CEJ region, providing insights into structural variations.

Optical coherence tomography (OCT) acquisition

OCT imaging was performed using the Callisto spectral-domain OCT system (Thorlabs Inc., New Jersey, USA), equipped with a superluminescent diode (central wavelength: 930 nm; bandwidth: 100 nm; maximum output power: 3 mW). The system provided axial and lateral resolutions of 5.3/7 µm (air/water) and 8 µm, respectively, with a penetration depth of 1.7 mm and sensitivity of 105 dB. The axial scanning frequency was 1.2 kHz, corresponding to approximately two volumetric images per second. For image acquisition, each B-scan consisted of 2000 A-scans, and each volumetric dataset was composed of 512 B-scans per sample, resulting in images of 2000 × 512 pixels. The lateral scanning length was adjustable up to 10 mm to fully cover the region of interest. Specimens were mounted on a PVC platform aligned to a fixed reference point, with micrometric positioning to maintain consistent orientation across acquisitions. Samples were imaged under four conditions: Group 1 (G1) – Air (control); Group 2 (G2) – Glycerol; Group 3 (G3) – Gold Nanorods (AuNRs) in water; and Group 4 (G4) – Gold Nanorods (AuNRs) in water combined with glycerol. Images were subsequently analyzed using ImageJ and OriginPro software.

Attenuation coefficient analysis

The regions of interests (ROIs) were selected in enamel, cementum, and the CEJ for comparative analysis. The ROIs were selected based on standardized window dimensions (10 A-scans) across all samples. For ROI placement, 'regular tissue' was defined as regions of enamel or cementum that appeared homogeneous and continuous in OCT images, without visible discontinuities, irregular interfaces, or signal voids, and confirmed by corresponding SEM/EDS analyses as structurally intact. 'Irregular tissue' was defined as CEJ regions exhibiting morphological variations such as enamel–cementum gaps, overlaps, or discontinuities, as evidenced by altered OCT signal intensity profiles (e.g., sharp drops, voids, or irregular scattering patterns).

The positioning of ROIs was adjusted per image to ensure that one window captured a regular reference area, and another captured an irregular CEJ variation. Using B-scan mode, the MATLAB software identified the tissue surface as a reference for A-scan normalization as shown in Fig. 1. For such data processing in MATLAB, three toolboxes were used including Image Processing Toolbox, Curve Fitting Toolbox, and Statistics and Machine Learning Toolbox. The normalized A-scan within each ROI was fitted to an exponential decay model using the Beer-Lambert law, yielding the attenuation coefficient (OAC) for further statistical analysis. For such calculations, the OCT signal intensity decay was recorded and was fitted using the Beer-Lambert law:

$$I(z) = I_0 e^{-\mu z} \quad (1)$$

Where $I(z)$ is the signal intensity at depth z, I_0 is the initial intensity. By fitting the intensity signal with this equation yielded the ' μ ' which is the OAC.

Statistical analysis

The calculated OAC data were derived from 20 extracted human teeth ($n=20$) that met the necessary inclusion criteria. The study employed a repeated-measures design where the extracted tooth served as the experimental unit. Each of the 20 teeth was subjected to all four treatment conditions (G1: Air, G2: Glycerol, G3: AuNRs, G4: AuNRs + water + Glycerol) sequentially.

The OAC was calculated for multiple ROIs within the Enamel, Cementum, and CEJ regions, with each OAC value derived from a standardized 10 A-scans at that location. The calculated OAC data were later analyzed using repeated-measures ANOVA and Tukey's post-hoc test ($p<0.05$). Statistical analyses were performed using R Studio (Version 2024.09.0).

Results

The OCT enabled the non-invasive identification of the CEJ along the cervical region of the tooth, revealing its subtypes and structural variations. To validate these findings, SEM was employed to examine surface morphology, while the EDS was used to analyze the molecular composition.

Morphology of cemento-enamel junction (CEJ)

To identify the interface between enamel and cementum, by OCT results, dehydrated samples were examined using scanning electron microscopy (SEM; Merlin Gemini II, Zeiss, Germany) at magnifications of 150x, 200x, 500x, 1000x, and 2000x, revealing well-defined structures in the CEJ region and a subtle transition between the tissues (Fig. 2).

Additionally, four types of tissue interrelations were observed: (1) Enamel over cementum; (2) edge-to-edge; (3) Gap between enamel and cementum; and (4) Cementum over enamel, corroborating the OCT observations. Microstructural characteristics, such as enamel porosity and fiber organization in the cementum, confirmed the anatomical variability present in the CEJ among samples and within the same tooth.

The EDS was employed to examine the molecular composition of the CEJ, focusing on the different typologies at the interface. Images were analyzed in three distinct regions: Cementum, Enamel, and the Cementoenamel Junction. The EDS spectral microanalysis detected peaks of calcium, phosphorus, carbon, and oxygen in the cementum, enamel, and CEJ regions. In the cementum, carbon and oxygen were more prevalent relative to calcium and phosphorus. In the enamel, calcium was predominant, while at the cementoenamel junction, high peaks of calcium and phosphate were observed, confirming the transitional composition between the dental layers (Figs. 3).

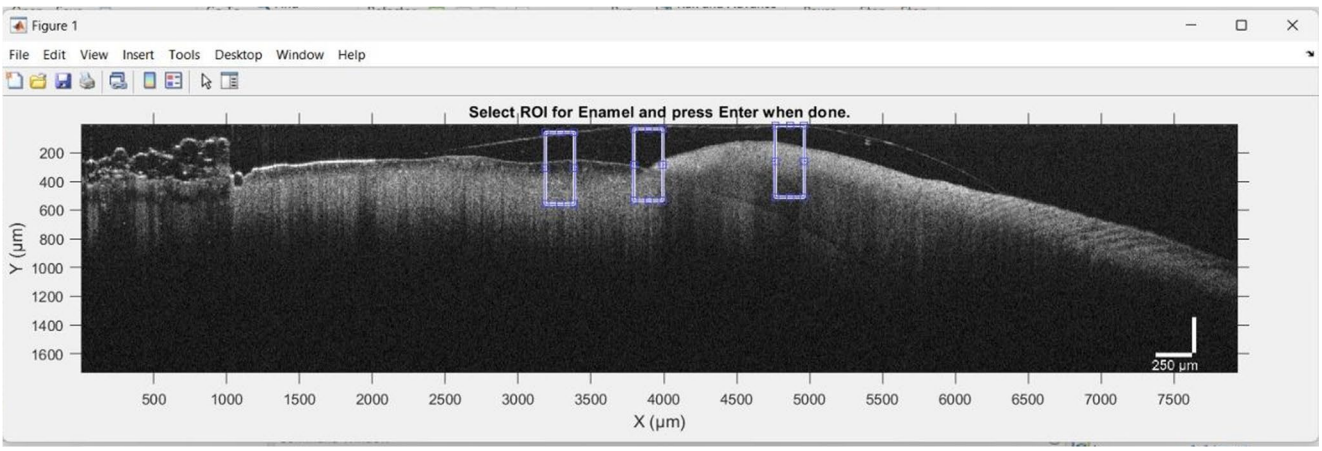

Fig. 1 Schematic of the working principle for obtaining the attenuation coefficients

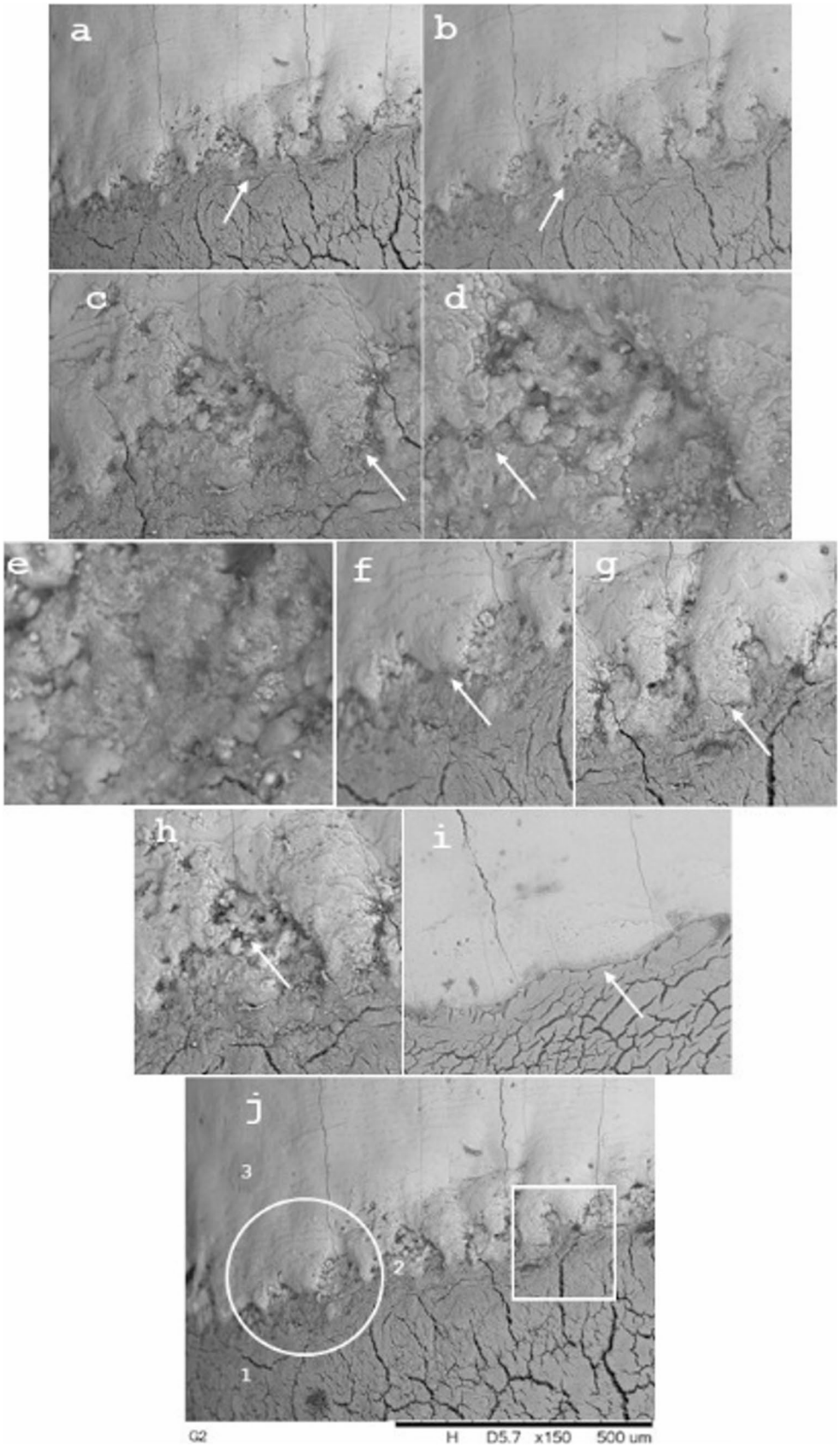

Fig. 2 Cemento-enamel junction (CEJ) visualized under scanning electron microscopy (SEM; Merlin Gemini II, Zeiss, Germany) at different magnifications: (**a**) 150×; (**b**) 200×; (**c**) 500×; (**d**) 1000×; (**e**) 2000×. CEJ morphologies observed: (**f**) enamel overlapping cementum; (**g**) cementum overlapping enamel; (**h**) gap between enamel and cementum; (**i**) edge-to-edge; (**j**) representative area showing enamel (circle), cementum (square), and dentin exposure. (**j**) (1) Cementum, (2) Dentin, (3) Enamel

Optical coherence tomography analysis

The correlation between Optical Coherence Tomography (OCT), Scanning Electron Microscopy (SEM), and Energy Dispersive Spectroscopy (EDS) enabled detailed characterization of the cementoenamel junction (CEJ). OCT images revealed significant differences in optical scattering behavior among the analyzed groups. Show the control group analyzed by OCT without nanoparticles, serving as a reference. This control group (G1) exhibited greater scattering and lower light penetration, resulting in less definition of the CEJ. The application of glycerol (G2) as an optical contrast agent enhanced definition, providing better visualization of the interface and revealing subtle morphological differences through alternating areas of higher and lower signal intensity Gold nanorods (G3) demonstrated higher brightness and reduced subsurface scattering. The fourth group (G4), combining gold nanorods diluted in glycerol, exhibited even lower scattering and a more continuous linear contour definition in the CEJ region (Fig. 4).

Table 1 presents the quantitative distribution of identifiable CEJ types in OCT samples, based on a total of 7,489 OCT images acquired from 20 teeth, each imaged under four experimental conditions (G1–G4: Air, Glycerol, AuNRs in water, and AuNRs in water + Glycerol). Each tooth was scanned at 20 μm intervals along the region of interest, generating approximately 126 B-scans per tooth. This systematic acquisition ensured complete coverage of the cementoenamel junction for all samples. The images were analyzed and categorized using Google Sheets®, with a descriptive analysis of the CEJ types. The table shows the absolute and relative frequencies of the different types, along with the means and standard deviations, with a 95% confidence interval for each category.

The introduction of glycerol (G2) showed a higher frequency (22.93%) of the Gap configuration (Type III) compared to the control group (G1) (11.60%). This increase suggests greater identification of gaps, reflecting consistency in their presence across samples. However, the use of glycerol did not have a statistically significant effect on this configuration. The mean of 37.25 for Type II, though lower than the negative control (74.9), presented a lower standard deviation (25.95), suggesting greater variability in the observations. For the Cement-over-enamel group (Type IV), the mean of 3.5 with glycerol (G2) was lower than the negative control (8.4), and the standard deviation of 7.99, higher than the mean, indicated high variability, reflecting a lower frequency but greater precision in identifying the CEJ characteristics.

When only gold nanorods (G3) were introduced, the CEJ of the edge-to-edge group (Type II) remained the most prevalent configuration, representing 49.38% of the images analyzed, although with a slightly lower frequency compared to the negative control (69.77%) and glycerol (50.24%). However, the contrast agents revealed a higher distribution of enamel over cementum (Type I) at 33.23% of the images, showing a frequency higher than that of the negative control (G1) and glycerol (G2). The frequency for the Cement-over-enamel group (Type IV) was 4.71%, with 95 occurrences, very close to that observed in the glycerol (G2) group (4.72%).

Fig. 3 Spectral microanalysis of EDS of cementum, enamel, and CEJ (cemento-enamel junction). Inset shows corresponding mas percentage of the elemental compositions (**a**) cementum, (**b**) enamel, (**c**) CEJ

When the contrast agents were mixed (G4), the frequencies of Types I and II of the CEJ were observed to be similar to those of the gold nanorods-only group (G3), although with slightly higher frequencies. The Lacuna (Gap) configuration (Type III) appeared more frequently (13.36% of the images), with 246 occurrences, showing a value higher than the gold nanorods-only group (G3) (8.68%). The frequency of Cement-over-enamel (Type IV) was 4.99%, with 92 occurrences, similar to that observed in the AuNRs + Water (G3) group (4.71%), glycerol (G2) group (4.72%), and the negative control group (G1) (7.81%). The small variation in frequency suggests that the AuNRs + Water mixture did not substantially alter the occurrence of Type IV, but may have improved its identification by highlighting less visible characteristics in air.

Quantitative analysis of CEJ attenuation coefficient with AuNRs contrast agent

The determination of the attenuation coefficient was categorized into three groups: Cement, Enamel, and the Cement-Enamel Junction in different dental samples. The goal was to verify whether the OCT images showed statistically significant differences in the attenuation coefficients within each contrast agent group. An analysis of variance (ANOVA) indicated statistically significant differences, and a Tukey post-hoc test identified which groups differed (Table 2).

In the analysis of the attenuation coefficients of the CEJ, the F-value of 6.804 with a p-value of 0.000401 indicated statistically significant differences between the groups. The Tukey test revealed that the G1 group (Negative Control - Air) had the highest average value (0.0015660), significantly differing from the G3 (AuNRs) and G4 (AuNRs + Water + Glycerol) groups, which were in group b. The G2 group (Glycerol) was intermediate (group ab), with an average value of 0.0012065. These results suggest that the attenuation coefficient was higher in the G1 group due to greater scattering. In contrast, the G3 and G4 groups exhibited optical properties favoring absorption, resulting in lower attenuation. Glycerol also contributed to lower

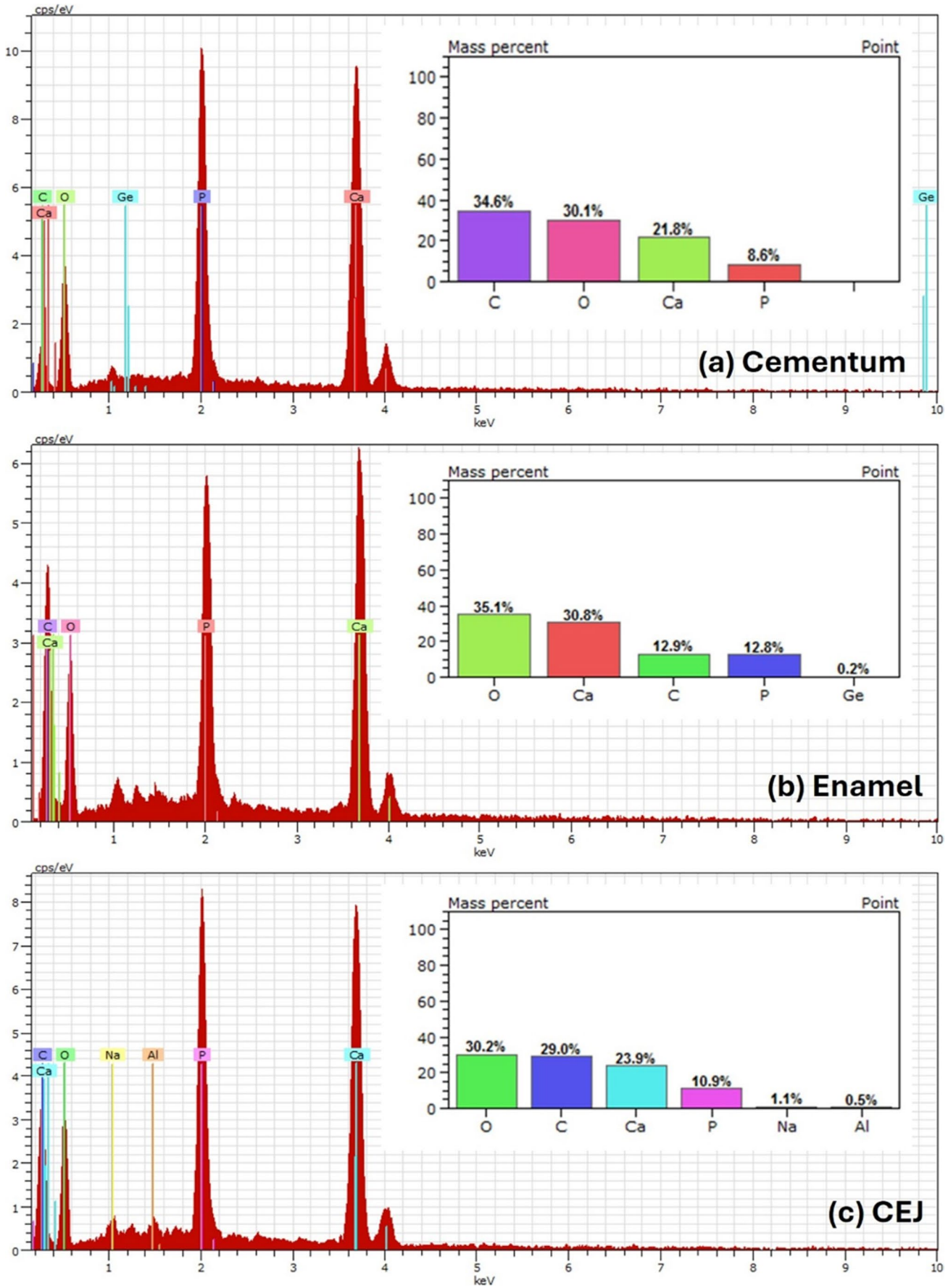
cps/eV
keV
C
O
Ca
Ge
P
Mass percent
Point
34.6%
30.1%
21.8%
8.6%
(a) Cementum
cps/eV
keV
C
O
Ca
P
Mass percent
Point
35.1%
30.8%
12.9%
12.8%
0.2%
(b) Enamel
cps/eV
keV
C
O
Ca
Na
Al
P
Mass percent
Point
30.2%
29.0%
23.9%
10.9%
1.1%
0.5%
(c) CEJ

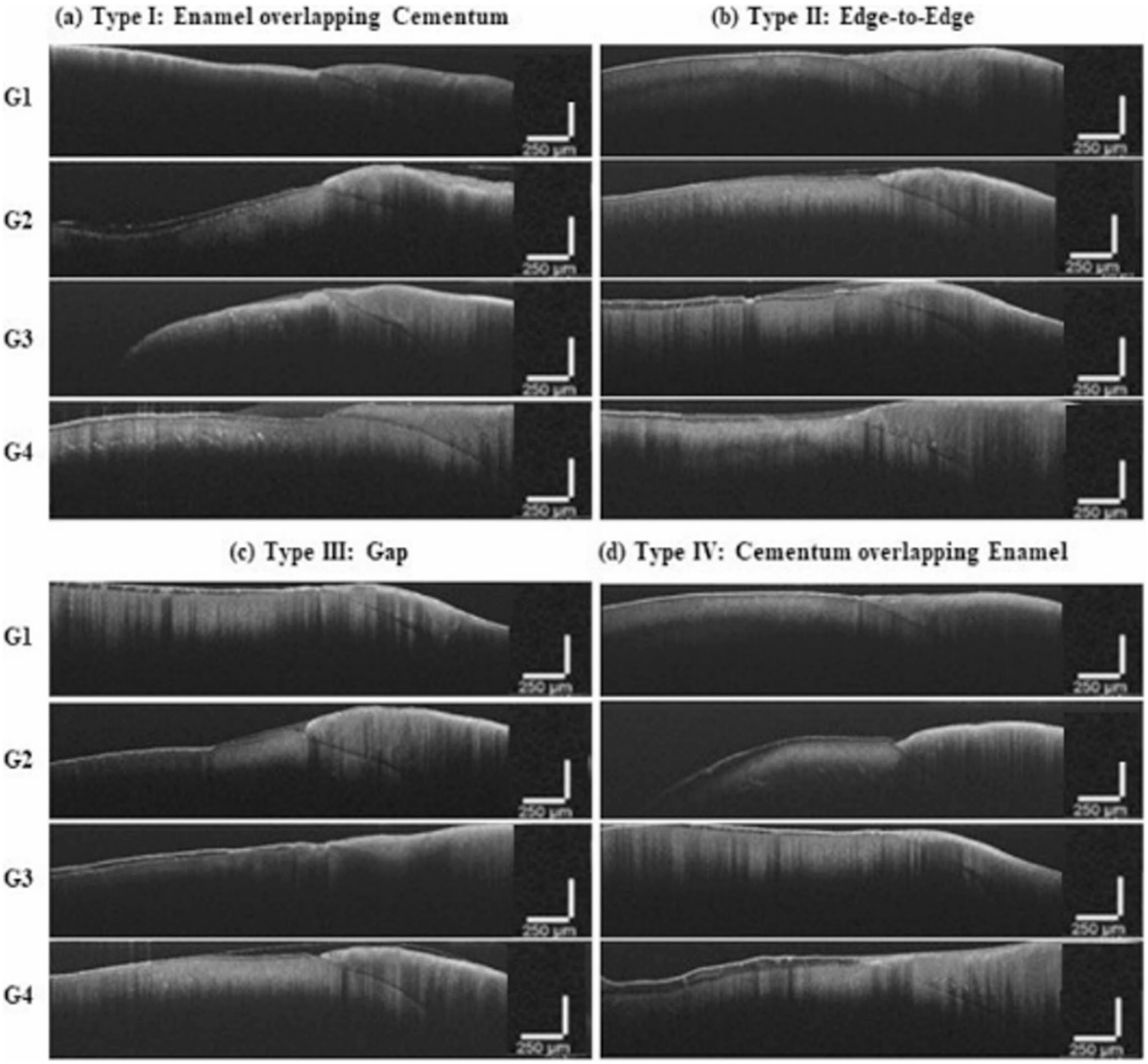

Fig. 4 Representative OCT images acquired with the TCO system (Thorlabs Inc., New Jersey, USA) illustrating four CEJ configurations: (**a**) Type I – enamel overlapping cementum, (**b**) (**b**) Type II – Enamel and cementum in edge-to-edge alignment,, (**c**) Type III – gap between enamel and cementum, and (**d**) Type IV – cementum overlapping enamel. Groups: (**A**) G1 – control (air), (**B**) G2 – glycerol, (**C**) G3 – gold nanorods (AuNRs), and (**D**) G4 – AuNRs + water + glycerol

attenuation, highlighting the contribution of absorption without predominating over scattering, but the attenuation was still lower than in the G3 and G4 groups.

In the analysis of the enamel attenuation coefficients, the F-value of 17.75 with a p-value of 7.94e-09 indicated statistically significant differences between the groups. The Tukey test showed that the G2 (Glycerol) and G1 (Negative Control - Air) groups had the highest average values (0.0019505 and 0.0017450, respectively), indicating no statistically significant difference between them. The G3 (AuNRs) and G4 (AuNRs + Water + Glycerol) groups had lower average values (0.0011100 and 0.0010435, respectively), with no significant differences between each other. However, there was a statistically significant difference between groups a and b, highlighting that the G2 and G1 treatments differ substantially from G3 and G4. This suggests that, in enamel, scattering was more pronounced in the Glycerol and Air groups, while the groups with AuNRs showed a lower scattering effect.

In the analysis of the attenuation coefficients of Cement, the F-value of 0.051 and the p-value of 0.985 indicated no statistically significant differences between the groups, as

Table 1 Mean and standard deviation (SD) of the sample sections categorized by the different types of CEJ analyzed in each group

Groups	CEJ patterns	Mean	SD
G1 (Air)	*Enamel overlapping cementum*	11.60	17.07
	Edge-to-edge	74.90	63.35
	Gap	12.45	18.81
	Cementum overlapping Enamel	8.40	16.86
G2 Glicerol	*Enamel overlapping cementum*	16.45	18.24
	Edge-to-edge	37.25	25.95
	Gap	17.00	19.49
	Cementum overlapping Enamel	3.50	7.99
G3 Aurods + Water	*Enamel overlapping cementum*	37.55	25.59
	Edge-to-edge	49.80	30.15
	Gap	8.75	16.74
	Cementum overlapping Enamel	4.75	8.47
G4 *Aurods + Water + Glicerol*	*Enamel overlapping cementum*	34.80	22.94
	Edge-to-edge	40.25	22.61
	Gap	12.30	19.16
	Cementum overlapping Enamel	4.60	5.76

the comparison was made based on an analysis of variance (ANOVA) and Tukey Test

Table 2 Multiple comparison of the Attenuation coefficients of the CEJ and its subtypes by the Tukey test. The values represent the mean ± standard deviation, and statistically significant differences were considered for $p < 0.05$

Anatomic Region	Group	Attenuation coefficient	Results
CEJ	*G1 – (Air)*	0.0015660	a
	G2 - Glicerol	0.0012065	ab
	G3 – Aurods + Water	0.0010830	b
	G4 - Aurods + Water + Glicerol	0.0009060	b
Enamel	*G1 – (Air)*	0.0019505	a
	G2 - Glicerol	0.0017450	a
	G3 – Aurods + Water	0.0011100	b
	G4 - Aurods + Water + Glicerol	0.0010435	b
Cementum	*G1 – (Air)*	0.001132	a
	G2 - Glicerol	0.001129	a
	G3 – Aurods + Water	0.001095	a
	G4 - Aurods + Water + Glicerol	0.001072	a

the p-value is much higher than the standard significance level of 0.05. In Table 2, the letter-based subgroup labels (a, b, ab) denote the results of the Tukey post-hoc test, which determined the statistical equivalence among the four treatment groups. Groups that share a letter are considered statistically equivalent ($p \geq 0.05$), while groups that do not share a letter exhibit a statistically significant difference ($p < 0.05$).

For the Cementum region specifically, the Tukey test reinforced the ANOVA conclusion by showing that all treatments (G1, G2, G3, and G4) belonged to the same statistical group (labelled 'a'), confirming the mean attenuation coefficients of all treatments were statistically equivalent in this tissue. This suggests that other factors, beyond the treatments investigated, may play a more relevant role in the observed variations.

Possible explanations include the intrinsic heterogeneity of the cementum, which presents variable degrees of mineralization and fiber organization across specimens, as well as technical aspects related to sample preparation and positioning during OCT acquisition.

Discussions

In this study, gold nanorods were used as contrast agents to enhance image clarity while preserving signal integrity and tissue structure in the CEJ. Using the OCT technique, the application of gold nanorods improved signal differentiation among CEJ morphologies without compromising optical quality. Arambawatta et al. [30] found the edge-to-edge pattern (Type II) predominates, which is consistent with our findings [30]. The gap (Type III) pattern showed a more uniform distribution in our study, unlike Arambawatta et al., where it was irregular and predominant. This may be due to the exclusive selection of premolars and small sample size.

The SEM-EDS results confirmed OCT images in identifying the CEJ, aligning with Hernández et al. (2020) [3]. Despite SEM-EDS being a high-resolution technique, its labor-intensive processing makes it impractical for clinical use. The OCT, however, allows non-invasive, real-time analysis, reinforcing its potential as a viable tool for periodontal diagnostics and structural evaluation.

Araveti et al. [10] conducted a similar study without optical clearing agents, identifying only three subtypes with different frequencies from our study [10]. The heterogeneity of dental tissues causes significant light scattering, affecting image quality and depth. Building on these challenges, this study evaluated the application of optical clearing agents, particularly AuNRs and glycerol, to reduce light scattering and improve image clarity. The AuNRs preserved image integrity and provided clearer visualization without compromising optical signal quality or tissue structure, as corroborated by Carneiro et al. (2024) [15].

The observed improvement in OCT contrast with AuNRs can be attributed to their localized LSPR properties [18, 19]. LSPR arises from the collective oscillation of conduction electrons at the nanoparticle surface when excited by incident light, resulting in enhanced local electromagnetic fields [24]. The resonance wavelength of AuNRs is highly

dependent on their aspect ratio, allowing precise tuning into the NIR range (700–1000 nm) [23]. This spectral tuning aligns with the low-absorption biological window, optimizing the interaction between the incident OCT light (930 nm in this study) and the nanoparticles. At resonance, AuNRs enhance both absorption and backscattering, which increases image contrast and reduces the relative contribution of multiple forward-scattering events that degrade OCT resolution [23].

Consequently, AuNRs amplify the OCT signal from tissue interfaces such as the CEJ, enabling improved delineation of structural boundaries compared with isotropic particles or untuned nanomaterials [15, 16]. We propose that these effects reflect a working theory for the improved contrast observed with AuNRs. The high light absorption and scattering capacity, biocompatibility, and potential protective effect against demineralization make the AuNRs promising optical clearing agent for enhancing imaging techniques like OCT.

Following this mechanistic explanation, we then analyzed the effect of AuNRs on the prevalence of CEJ configurations across groups. The analysis of groups (G3) AuNRs and (G4) AuNRs + Water + Glycerol revealed the edge-to-edge configuration was most prevalent, consistent with Arambawatta et al. (2009) [30] and Avareti et al. (2019) [10]. However, Metwally et al. [2] found the enamel over cementum type most prevalent using SEM, suggesting inspection methodology influences detection and quantification. This study employed a non-invasive imaging technique suitable for clinical use [2].

The enamel over cementum (Type I) configurations increased in groups containing AuNRs (G3 and G4) due to gold's plasmonic resonance wavelength being close to enamel's refractive index. The lower prevalence of the cementum over enamel subtype contrasts with Adhikari et al. (2024) [1]. Differences may be due to genetic diversity, sample origin, and environmental factors. The edge-to-edge type was followed by enamel over cementum, gap and cementum over enamel. High variability in standard deviations reflects anatomical diversity. The presence of lacunae in the CEJ is a risk factor for plaque retention, increasing susceptibility to periodontal diseases. The rare cementum over enamel type poses clinical challenges due to potential dentin exposure.

The attenuation coefficient calculation showed AuNRs + Water + Glycerol (G4) and AuNRs + Water (G3) groups had less light scattering compared to the air (G1). This aligns with Fan et al. [31], highlighting gold nanoparticles' superior optical properties [31]. AuNRs enhance light penetration and image contrast, especially when combined with glycerol, demonstrating a synergistic effect.

A recent literature review [De Lima et al., 2025] indicates that no studies have identified the use of gold nanoparticles for enhancing imaging in this cervical region of the tooth [32]. This underscores the importance of the present ex vivo study as a starting point for further investigations into this critical interface for periodontal and rehabilitative approaches to the root and coronal portions.

One limitation of this study is the lack of detailed background information for the extracted teeth, including causal factors for tooth loss. Additionally, the periodontal history of the donors was unavailable, which could influence CEJ morphology. To minimize this limitation, a rigorous debridement protocol was applied to remove surface irregularities and preserve the cemento-enamel junction for accurate imaging. Furthermore, special attention was given to sample selection, ensuring that all extracted teeth had been stored for no longer than six months, since prolonged storage in biobanks may alter tissue preservation over time. Future studies should aim to collect more detailed etiological information on the samples, allowing for potential correlations between CEJ characteristics and factors such as age and gender.

Given its vulnerability, future studies may expand this analysis using more complex biological models, aiming for improved clinical applicability. Despite challenges with agent flow, this study demonstrated that AuNRs significantly enhanced the CEJ visualization in OCT, overcoming diagnostic limitations. Our results showed that the AuNR-containing groups (G3 and G4) exhibited the lowest attenuation coefficients in the CEJ regions, suggesting that these agents possess optical properties that favor absorption while markedly reducing light scattering.

The superior performance of the G4 group (AuNRs combined with glycerol) over G2 (glycerol only) can be attributed to a synergistic effect. The superior performance of the G4 group (AuNRs combined with glycerol) can be attributed to a synergistic effect. The AuNRs used in this study had an average length of 68 nm, diameter of 11.7 nm, and an aspect ratio of 5.3, which corresponds well to a LSPR peak near 930 nm. This close spectral overlap with the OCT system wavelength (930 nm) optimized contrast and signal enhancement. Such tunability of the LSPR with nanorod aspect ratio is well documented, with prior studies confirming that aspect ratios around 5 typically red-shift the plasmon resonance into the 900–950 nm range, consistent with our findings [33, 34].

In parallel, glycerol (RI ≈ 1.47) acted as a potent optical clearing agent, infiltrating the tissue to achieve better RI matching (dental enamel IR ~ 1.62) and drastically reducing bulk scattering. Although increased absorption typically raises the total attenuation coefficient, in highly scattering

tissues such as dental enamel, attenuation is primarily governed by the scattering coefficient. Thus, the lower overall attenuation observed in the AuNR groups (G3 and G4) is not contradictory. Rather, it demonstrates that the substantial reduction in bulk scattering - achieved through the optical clearing effect - far outweighed the modest increase in absorption introduced by the AuNRs. This net positive effect underscores the effectiveness of AuNRs in enhancing light penetration and signal detection.

Collectively, these findings support the clinical application of AuNRs to improve OCT resolution and manage dental treatment planning effectively. Future research should transition from ex vivo to in vivo studies, focusing on the safety, biocompatibility, and optimized delivery of AuNRs for clinical use. It is crucial to evaluate their long-term effects on image quality and diagnostic accuracy across diverse dental tissues and patient populations, while also addressing challenges in agent flow to ensure consistent and effective application in clinical settings.

Conclusions

This study demonstrated the efficacy of gold nanorods (AuNRs) as contrast agents for enhancing the visualization of the cementoenamel junction (CEJ) in optical coherence tomography (OCT). The comparative analysis with scanning electron microscopy (SEM) and energy-dispersive X-ray spectroscopy (EDS) confirmed the identification of four prevalent configurations, with the edge-to-edge configuration being the most common, validating OCT as a non-invasive and real-time diagnostic tool. Qualitative and quantitative assessments revealed that AuNRs effectively highlighted the CEJ interfaces by reducing scattering and increasing brightness, particularly for the Gap configuration, which poses the greatest clinical challenge due to its vulnerability to attacks from the oral environment. The combination of these contrast agents significantly improved the definition and visualization of the CEJ interfaces. Furthermore, the attenuation coefficient analysis indicated greater image definition in enamel and the CEJ with AuNRs, although no statistically significant differences were observed in the cementum. These findings underscore the potential of AuNRs to enhance OCT imaging, offering a promising approach for periodontal diagnostics and structural evaluation in clinical practice. Future research will explore the broader application of these contrast agents in various dental tissues and their long-term effects on image quality and diagnostic accuracy.

Supplementary Information The online version contains supplementary material available at https://doi.org/10.1007/s10103-025-04735-x.

Acknowledgements We thank the University of Pernambuco, Coordination for the Improvement of Higher Education Personnel (CAPES) - Grant number 001, and the Foundation for the Support of Science and Technology of the State of Pernambuco (FACEPE)—APQ 1354-4.02/22.

Author contributions C.P.S. and M.H.C.T.L. wrote the main manuscript text. M.B.S.J. and M.R.N.C. contributed to sample preparation and data acquisition. A. N. A., A.D., M.P., D. F. T. S. and D. M. Z. assisted with experimental procedures, expertise in imaging analysis and contributed to data interpretation and supervised the experimental design and revised the manuscript. A.S.L.G. provided critical feedback and contributed to the discussion. D.S.L. coordinated the project and finalized the manuscript. All authors reviewed and approved the final version of the manuscript.

Funding The authors declare that this study was funded by the Coordination for the Improvement of Higher Education Personnel (CAPES, Grant 001) and the Foundation for the Support of Science and Technology of the State of Pernambuco (FACEPE, Grant APQ 1354 − 4.02/22).

Data availability No datasets were generated or analysed during the current study.

Declarations

Competing interests The authors declare no competing interests.

References

1. Adhikari BR et al (2023) Cementoenamel junction: morphological characterization in Nepali population. J Nepal Soc Periodontol Oral Implantol 7(2):50–54
2. Metwally S, Stachewicz U (2020) Teeth resorption at cement - enamel junction (CEJ) - microscopy analysis Micron 137:102913. https://doi.org/10.1016/j.micron.2020.102913 https://doi.org/10.1016/j.micron.2020.102913
3. Hernández SZ et al (2020) Morphology of the cementoenamel junction in permanent teeth of dogs: a scanning electron microscopic study. J Vet Dent 37(3):159–166
4. Arambawatta K et al (2021) Morphological analysis of cementoenamel junction in premolars of Sri Lankans. Anat Sci Int 96(4):509–516
5. Lanning SK et al (2005) Variation in periodontal diagnosis and treatment planning among clinical instructors. J Dent Educ 69(3):325–337
6. Barendregt DS et al (2009) Detection of the cemento-enamel junction with three different probes: an in vitro model. J Clin Periodontol 36(3):212–218
7. Baek JH (2024) Potential application of non-invasive optical imaging methods in orthodontic diagnosis. J Clin Med 13(4):966
8. Fleiner J et al (2013) Digital method for quantification of circumferential periodontal bone level using cone beam CT. Clin Oral Invest 17:389–396
9. Nguyen K-CT et al (2016) Imaging the cemento-enamel junction using a 20-MHz ultrasonic transducer. Ultrasound Med Biol 42(1):333–338
10. Araveti Sk et al (2020) Swept-source optical coherence tomographic observation on prevalence and variations of cementoenamel junction morphology. Lasers Med Sci 35:213–219
11. Maia AMA et al (2016) Evaluation of dental enamel caries assessment using quantitative light induced fluorescence and optical coherence tomography. J Biophotonics 9(6):596–602

12. Tsai M-T et al (2019) Early detection of enamel demineralization by optical coherence tomography. Sci Rep 9(1):17154
13. Haak R et al (2019) Clinical and OCT outcomes of a universal adhesive in a randomized clinical trial after 12 months. J Dent 90:103200
14. Larin KV et al (2011) Optical clearing for OCT image enhancement and in-depth monitoring of molecular diffusion. IEEE J Sel Top Quantum Electron 18(3):1244–1259
15. Carneiro VSM et al (2024) Optical clearing agents based on metallic and dielectric nanoparticles for caries diagnostic by optical coherence tomography. Clin Oral Invest 28(1):72
16. Das A et al (2022) Exploiting nanomaterials for optical coherence tomography and photoacoustic imaging in nanodentistry. Nanomaterials 12(3):506
17. Yang VB, Curtis DA, Fried D (2018) Use of optical clearing agents for imaging root surfaces with optical coherence tomography. IEEE J Sel Top Quantum Electron 25(1):1–7
18. Bansal SA et al (2020) Role of gold nanoparticles in advanced biomedical applications. Nanoscale Adv 2(9):3764–3787
19. Wang A et al (2022) Molecular contrast optical coherence tomography and its applications in medicine. Int J Mol Sci 23(6):3038
20. Singh RP, Ramarao P (2012) Cellular uptake, intracellular trafficking and cytotoxicity of silver nanoparticles. Toxicol Lett 213(2):249–259
21. Derfus AM, Chan WC, Bhatia SN (2004) Probing the cytotoxicity of semiconductor quantum dots. Nano Lett 4(1):11–18
22. Link S, El-Sayed MA (1999) Size and temperature dependence of the plasmon absorption of colloidal gold nanoparticles. J Phys Chem B 103(21):4212–4217
23. Jain PK et al (2006) Calculated absorption and scattering properties of gold nanoparticles of different size, shape, and composition: applications in biological imaging and biomedicine. J Phys Chem B 110(14):7238–7248
24. Pisano F et al (2024) Potential of plasmonics and nanoscale light–matter interactions for the next generation of optical neural interfaces. Neurophotonics 11(S1):S11513–S11513
25. Murphy CJ et al (2008) Gold nanoparticles in biology: beyond toxicity to cellular imaging. Acc Chem Res 41(12):1721–1730
26. Alkilany AM, Murphy CJ (2010) Toxicity and cellular uptake of gold nanoparticles: what we have learned so far? J Nanopart Res 12(7):2313–2333
27. Topala F et al (2021) En-face optical coherence tomography analysis of gold and silver nanoparticles in endodontic irrigating solutions: an in vitro study. Exp Ther Med 22(3):992
28. Wei M-Z et al (2021) Seed-mediated synthesis of gold nanorods at low concentrations of CTAB. ACS Omega 6(13):9188–9195
29. Nicolae CL, Pîrvulescu DC, Antohi AM, Niculescu AG, Grumezescu AM, Croitoru GA (2024) Silica nanoparticles in medicine: overcoming pathologies through advanced drug delivery, diagnostics, and therapeutic strategies. Rom J Morphol Embryol 65(2):173–184. https://doi.org/10.47162/RJME.65.2.03
30. Arambawatta K, Peiris R, Nanayakkara D (2009) Morphology of the cemento-enamel junction in premolar teeth. J Oral Sci 51(4):623–627
31. Fan Y et al (2024) Green synthesis of biocompatible chiral gold nanoparticles. Polymers 16(23):3333. https://doi.org/10.3390/polym16233333
32. de Lima MHDT et al (2025) Unraveling applications of gold nanoparticles in dentistry: a scoping review. J Dent 156:105685. https://doi.org/10.1016/j.jdent.2025.105685
33. Takahata R et al (2018) Gold ultrathin nanorods with controlled aspect ratios and surface modifications: formation mechanism and localized surface plasmon resonance. J Am Chem Soc 140(21):6640–6647
34. Cavigli L et al (2021) Photostability of contrast agents for photoacoustics: the case of gold nanorods. Nanomaterials 11(1):116

Authors and Affiliations

Carolina Pereira Da Silva[1] · Maria Heloísa da Conceição Tavares de Lima[1] · Manoel Bernardo da Silva Júnior[1] · Marcela Rosa Nogueira Cavalcanti[1] · Audrey Nunes de Andrade[2] · Avishek Das[3] · Manojit Pramanik[3] · Daniela De Fátima Teixeira Da Silva[4] · Denise Maria Zezell[4] · Anderson Stevens Leônidas Gomes[5] · Daniela Siqueira Lopes[1]

✉ Daniela Siqueira Lopes
daniela.siqueira@upe.br

Carolina Pereira Da Silva
carolina.pereira@upe.br

Maria Heloísa da Conceição Tavares de Lima
mheloisa.tavareslima@upe.br

Manoel Bernardo da Silva Júnior
manoel.bernardo@upe.br

Marcela Rosa Nogueira Cavalcanti
marcela.rncavalcanti@upe.br

Audrey Nunes de Andrade
audrey.andrade@cetene.gov.br

Avishek Das
avishek@iastate.edu

Manojit Pramanik
mano@iastate.edu

Daniela De Fátima Teixeira Da Silva
dfteixeira@alumni.usp.br

Denise Maria Zezell
zezell@usp.br

Anderson Stevens Leônidas Gomes
anderson.lgomes@ufpe.br

[1] Universidade de Pernambuco, Recife, Brazil

[2] Centro de Tecnologias Estratégicas do Nordeste, Recife, Brazil

[3] Iowa State University, Ames, United States

[4] Instituto de Pesquisas Energéticas e Nucleares, São Paulo, Brazil

[5] Federal University of Pernambuco, Recife, Brazil